Identification of Active Sites of Biomolecules. 1. Methyl-α-mannopyranoside and Fe^{III}

Orkid Coskuner,*,†,‡ Denis E. Bergeron,† Luis Rincon,†,§ Jeffrey W. Hudgens,† and Carlos A. Gonzalez†

Computational Chemistry Group, Physical and Chemical Properties Division, National Institute of Standards and Technology, 100 Bureau Drive, Mail Stop 8380, Gaithersburg, Maryland 20899, Computational Materials Science Center, George Mason University, Research I, Fairfax, Virginia 22030, and Departamento de Química, Universidad de los Andes, Mérida-5101, Venezuela

Received: December 14, 2007; In Final Form: January 17, 2008

Car−Parrinello molecular dynamics (CPMD) simulations, DFT chemical reactivity index calculations, and mass spectrometric measurements are combined in an integrated effort to elucidate the details of the coordination of a transition-metal ion to a carbohydrate. The impact of the interaction with the Fe^{III} ion on the glycosidic linkage conformation of methyl-α-D-mannopyranoside is studied by classical molecular dynamics (MD) and CPMD simulations. This study shows that Fe^{III} interacts with specific hydroxyl oxygen atoms of the carbohydrate, affecting the ground state carbohydrate conformation. These conformational details are discussed in terms of a set of supporting experiments involving electrospray ionization mass spectrometry, and CPMD simulations clearly indicate that the specific conformational preference is due to intramolecular hydrogen bonding. Classical MD simulations proved insensitive to these important chemical properties. Thus, we demonstrate the importance of chemical reactivity calculations and CPMD simulations in predicting the active sites of biological molecules toward metal cations.

I. Introduction

The development of experimental and theoretical techniques for identifying and predicting structure−function relationships in biological and biometallic molecular systems is of critical importance to basic and applied biochemical research. An accurate description of the active sites of biological molecules, for example, peptides and saccharides, and of reaction mechanisms relevant to physiological processes—receptor and ligand binding—may be achieved through coordinated experimental and computational efforts. In this work, we describe an integrated approach which utilizes theoretical calculations, molecular dynamics simulations, and mass spectrometry measurements to identify the active sites of a biomolecule. We have treated the metal−organic complex formed from the Fe^{III} ion and methyl-α-D-mannopyranoside as a representative example of a broad class of interesting saccharide−metal (Sac−Met) complexes.

Saccharides are ubiquitous in biological and ecological systems, and the presence of multi-hydroxyl functionality and well-defined stereochemistry make them potential ligands for metal coordination; the resulting inorganic complexes play important roles in diverse processes. Saccharide complexation with iron ions produces bioavailable species of iron suitable for nutritional supplementation.[1,2] Iron nanoparticles and their complexes with saccharides have recently been used in new treatment strategies in regenerative medicine as biomarkers (stem cell labeling).[3,4] Microbial saccharides are known to scavenge iron particles and to induce crystallization of unexpected phases such as nontronite,[5] which is an iron-rich clay mineral. Iron deficiency causes bacterial pathogens, which involve saccharides attached to the cell surface, to produce greater tissue damage since many virulence factors are determined by the iron supply.[6] Despite the importance of saccharide−iron (Sac−Fe) complexes in many processes, the reaction of iron with saccharides is poorly understood. Understanding this reaction is of great interest for designing, engineering, and synthesizing new Sac−Fe complexes that can be used as catalysts, novel materials, drugs, and biomarkers.

Studies involved with the structure of Sac−Fe complexes pose a challenge due to the possibility of multidentate coordination of the metal ion and the many degrees of freedom present in saccharides. Furthermore, accurate predictions of the structure, conformation, and coordination of Sac−Met's are immensely challenging due to the fast dynamics. Ever since the pioneering experimental work of Saltman in the 1960s regarding the Sac−Fe complexes,[7−9] and the studies on sugar chelating ability by Davis and Deller,[10] there has been a large gap in the literature regarding the understanding of these metal−organic complexes. A recent exception is the study by Rao et al.,[11] who proposed synthetic strategies for the isolation, characterization, and stabilization of Sac−Met species, including those of iron. Some recent work suggests that electrospray ionization (ESI) techniques enable mass spectrometry to shed new light on these complexes. Electrospray ionization mass spectrometry (ESI-MS) overcomes the time scale problems of nuclear magnetic resonance spectroscopy and the solubility problems of crystallographic techniques.[12] Sampling the distribution of ions directly from solution, ESI captures transient inorganic complexes, so that unique chemical insights are afforded. Sac−Met complexes in particular have been studied via ESI,[13−16] primarily as a means to stereochemical differentiation; when metal atoms are used as cationizing agents, the different sterioisomeric monosaccharides give different fragmentation patterns in collision-

* To whom correspondence should be addressed. E-mail: orkid.coskuner@nist.gov.
† National Institute of Standards and Technology.
‡ George Mason University.
§ Universidad de los Andes.

10.1021/jp711759q CCC: $40.75
Published on Web 02/27/2008

induced dissociation (CID) experiments. While these experiments do give some rudimentary insight as to coordination, they cannot describe the reactivity and reaction mechanisms at the electronic level. A clear understanding of the impact of transition-metal ion interaction on the preferred conformation of the saccharide and the chemical reactivity of the saccharide toward more than one transition-metal ion is desirable and may potentially be accessed through the theoretical strategies outlined herein.

In general, theoretical studies have been useful in modeling the complexation of metal ions with organic species. An example is the classical molecular dynamics study of the UDP-glucose interactions with magnesium cations by Petrova et al.[17] Most recently, Krewulak et al. studied the dynamics of the periplasmic ferric hydroxamate binding protein using classical simulations.[18] Static first-principles calculations, including density functional theory (DFT), have been applied to study the coordination and conformation of metal−organic species. Sillanpaa et al. used DFT calculations to conclude that the complexation of polycarboxylic acids with calcium, manganese, iron, zinc, and magnesium ions depends strongly on the particular metal ion (see ref 19 for details).

It is widely believed that the conformation of a carbohydrate is determined by steric factors and hydrogen-bonding interactions. Static first-principles calculations that attempt to solve the Schrödinger equation either using ab initio methods or by utilizing semiempirical methods that use approximations of the electronic interactions cannot capture the dynamical impact of the metal ion on the conformation of the biomolecule. Even though classical molecular simulation studies of organic and bioorganic molecules are firmly established and allow thorough dynamic investigations, their application in organometallic chemistry is complicated. An accurate representation of partially filled orbitals (d orbitals) that allows studies of possible coordination geometries and the chemistry of transition-metal complexes needs to be achieved. Furthermore, prediction of the types of bonding (particularly π bonding) between organic molecules and metal ions is difficult within classical molecular simulations. The accuracy of classical molecular simulation results depends strongly on the quality of interaction potential functions. Difficulties achieving accurate results for saccharides using classical simulations have been reported, for example, incorrect representation of the $\sigma(1 \rightarrow 6)$-linked saccharides.[20,21] Potential functions are typically based on pairwise additive interactions, and inclusion of higher-order terms is usually limited to two- or three-body terms. Potential functions derived in this manner usually overestimate the binding energy of the biomolecule and ignore nonadditive polarization behavior.

Encouraged by recent successful ab initio molecular dynamics simulations of transition-metal ions and biomolecules,[22−25] we studied the preferred glycosidic linkage orientation of methyl-α-D-mannopyranoside and how it changes upon interaction with Fe^{III} ions. Car−Parrinello molecular dynamics (CPMD) simulations were compared to classical MD simulations. We deploy here a theoretical strategy based on various ab initio techniques—CPMD simulations, chemical reactivity index, and partial charge analysis—to tackle the coordination chemistry problem of metal−organic species. We predict the number of transition-metal ions coordinated to the biomolecule and the structure and conformation of the biomolecule−transition-metal complexes. Results obtained using the collective ab initio techniques are then compared to those obtained via classical simulations and checked for consistency with the results of collision-induced dissociation (CID) experiments.

Both CPMD and classical MD simulations show that the conformational preference of the glycosidic linkage of methyl-α-D-mannopyranoside is ordered gauche clockwise (g+) > gauche anticlockwise (g−) > trans (t) in the gas phase. Upon coordination of Fe^{III}, this trend becomes g+ > t ≈ g− with the CPMD simulations, whereas classical MD simulations detect no change in the original trend. Specifically, our ab initio studies suggest that intramolecular hydrogen bonds stabilize the g+ conformation of the glycosidic linkage of methyl-α-D-mannopyranoside over its g− and t orientations; classical MD simulations were insensitive to this effect. Furthermore, our ab initio calculations are consistent with experimental results in suggesting that only one Fe^{III} ion coordinates to the methyl-α-D-mannopyranoside. We suggest that the integrated experimental and computational (including theory and simulation) approaches described herein may be useful in the chemical description of a broad range of important biometallic systems.

II. Methods Section

A. Car−Parrinello Molecular Dynamics Simulations. All CPMD simulations were performed with the NWCHEM program.[26,27] The Becke−Lee−Yang−Parr (BLYP) gradient-corrected functional, found to be reliable in describing methyl-β-mannose and glucose, was used along with the Troullier−Martins pseudopotentials and a double-ζ basis set.[28,29] The electronic wave functions were expanded in a plane wave basis set with a kinetic energy cutoff of 114 Ry. A homogeneous background charge was applied to compensate for the ionic charge. The time step for the simulation was set to 0.1 fs, and the electronic mass was set to 900 au. The isotopic mass of deuterium was used for hydrogen.

Simulations for 80 ps were performed for methyl-α-D-mannopyranoside (M), methyl-α-D-mannopyranoside−Fe^{III} (M−Fe^{III}), and methyl-α-D-mannopyranoside−Fe^{III}_2 (M−Fe^{III}_2) in the gas phase. Statistics were collected for the last 70 ps. Separate CPMD simulations of M and its complexes with Fe^{III} ions were performed in cubic cells with lattice parameters of 25, 35, and 45 Å with periodic boundary conditions. It was found that these lattice parameters do not have a significant impact on the predicted structural and thermodynamic results. Canonical ensemble CPMD simulations were performed at room temperature using the Nose−Hover thermostat. Long-range interactions were treated with the Ewald sum method.

B. Classical Molecular Dynamics Simulations. All classical MD simulations were performed using the NAMD program.[30] The OPLS-AA and UFF parameters were chosen for the carbohydrate and the metal ions, respectively.[31,32] The Lorentz−Berthelot mixing rules were applied for calculating the cross parameters. Separate canonical ensemble simulations for 60 ns were performed for M and its complexes with Fe^{III} ions. Statistics were collected for the last 50 ns. Homogeneous background charge was applied to compensate for the ionic charge. For these studies, the cubic box lengths of 25, 35, and 45 Å were chosen using periodic boundary conditions to study the effect of the box length on the predicted results. It was found that these chosen box lengths do not impact the predicted classical simulation results. Long-range interactions were treated with the Ewald sum method, and the simulations were coupled to an external bath at 300 K using the Langevin dynamics.[33]

C. Determination of the Conformational Preference of the Glycosidic Linkage. Figure 1 illustrates the structure of M along with the numbering of specific heavy atoms. The glycosidic linkage defined by the torsional angle φ = O5−C1−O1−C7 was varied from 0 to 360° to study the relative torsional energies

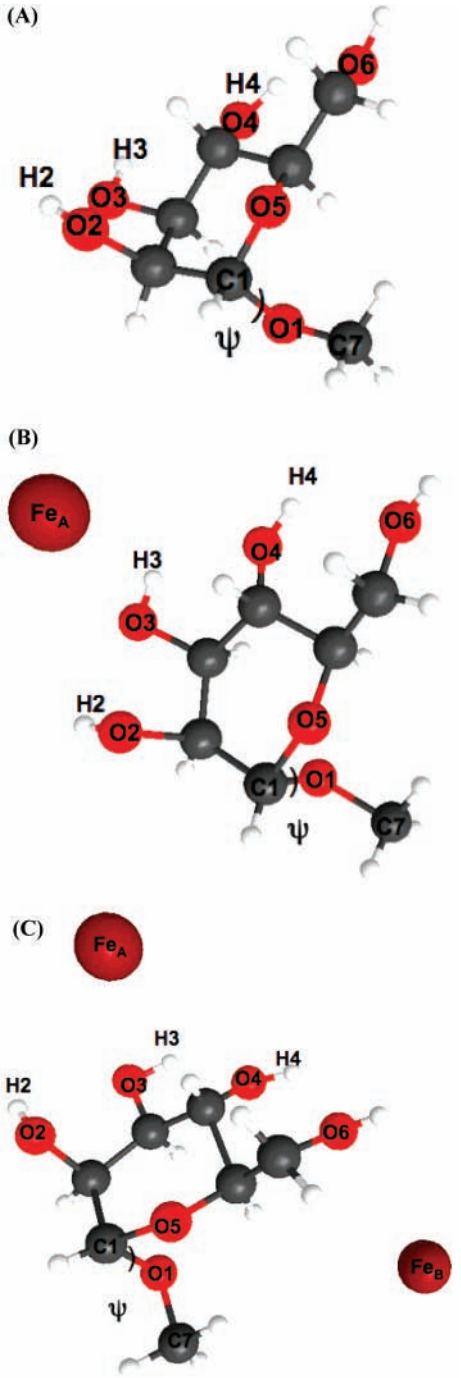

Figure 1. The methyl-α-D-mannopyranoside molecule (A) and its complexes with one and two Fe^{III} ions (B, C), obtained from CPMD simulations, with the conventional numbering of atoms.

in the gas phase. Following the recent successful applications of the potential of mean force (PMF) method on carbohydrates and metal−organic complexes using CPMD and classical MD simulations,[22,23,25] we determined the PMF of the glycosidic linkage of M in the gas phase and in the presence of Fe^{III} ions utilizing eq 1[33]

$$\Delta G = -kT \ln Z \tag{1}$$

where Z is the probability of the torsional angle of the glycosidic linkage between 0 and 360° obtained by CPMD and classical MD simulations. For the CPMD simulations ($\lambda = 0 \rightarrow \lambda = 1$, where $\lambda = 0$ and 1 are the initial and final states), the system was simulated for 80 ps for each window. To establish the adequacy and the convergence of PMF, we compared the PMF values calculated for $\lambda = 0 \rightarrow \lambda = 1$ to those obtained for $\lambda = 1 \rightarrow \lambda = 0$. We found that the PMFs exhibit the same profiles. Furthermore, we compared the PMFs to the results obtained from 50, 60, and 70 ps simulations for each window. The standard deviation in PMF was computed using the results obtained from these different CPMD simulation times. For the classical MD simulations, the system was simulated for 800 ps for each window, and the convergence was tested via comparing the PMF results for $\lambda = 0 \rightarrow \lambda = 1$ to those obtained for $\lambda = 1 \rightarrow \lambda = 0$. We also compared the PMFs to the results obtained from 500, 600, and 700 ps simulations for each window. The standard deviation was also calculated using these different classical MD simulation times. The observed deviations from the PMF ($\lambda = 0 \rightarrow \lambda = 1$ and $\lambda = 1 \rightarrow \lambda = 0$) for various simulation times do not exhibit any definite trends, indicating that the system is equilibrated and exhibits statistical fluctuations around the average PMF profile determined by both CPMD and classical MD simulations.

In addition, the perturbation method was employed, and the free-energy change between two states, l and $l + 1$, with the Hamiltonians H_l and H_{l+1} was computed using eq 2[33]

$$\Delta G(\lambda_{l+1} - \lambda_l) = -kT \ln\langle \exp[-(H_{\lambda_{l+1}} - H_\lambda)/kT]\rangle_{\lambda_l} \tag{2}$$

where λ is a continuous coupling parameter that represents $\lambda = 0$ and 1 as the initial and final states. Perturbations were broken into a series of intermediate states (20 steps with a $\Delta\lambda$ value of 0.05) in which the energy difference did not exceed the kT value, where k is the Boltzmann constant and T is the temperature. Results were compared to those obtained via PMF calculations.

D. Chemical Reactivity Index. In order to identify the sites in the substrate M more likely to bind to metal ions, we have performed a chemical reactivity analysis of these systems based on calculations of the Fukui reactivity indexes. The Fukui functions,[34] $f(\vec{r})$, provide a robust and efficient way to capture the physics governing chemical reactivity. Within the DFT formalism, the Fukui function (FF) is defined as[34]

$$f(\vec{r}) = \left[\frac{\delta\mu}{\delta v(\vec{r})}\right]_N \tag{3}$$

where μ is the chemical potential, $v(\vec{r})$ is the external potential, and N is the total number of electrons. Applying Maxwell's relations of the derivatives and assuming that the total energy of a molecular system is a function of N, eq 3 becomes

$$f(\vec{r}) = \left[\frac{\partial\rho(\vec{r})}{\partial N}\right]_v \tag{4}$$

where $\rho(\vec{r})$ is the electron density. In the frozen orbital approximation,[35] the FF becomes equal to the Kohn−Sham frontier orbital density, and the following functions can be defined as[36]

$$f^v(\vec{r}) = |\phi^v(\vec{r})|^2 \tag{5}$$

where v = HOMO or LUMO and $\phi^v(\vec{r})$ is the corresponding Kohn−Sham frontier molecular orbital. When v = HOMO (LUMO), eq 5 quantifies the susceptibility of the molecule

toward electrophilic (nucleophilic) attacks. A measure of the susceptibility toward radical attacks is given by

$$f^{\mathrm{rad}}(\vec{r}) = \frac{(f^{\mathrm{HOMO}}(\vec{r}) + f^{\mathrm{LUMO}}(\vec{r}))}{2} \quad (6)$$

Contreras et al.[37] have developed a method that allows one to compute these values condensed to a particular atom *i* on the molecule. According to this method, the condensed Fukui function at an atom *i* is given by

$$f_i^{\nu} = \sum_{\mu \in i}^{\mathrm{AO}} \left[|c_{\mu\nu}|^2 + c_{\mu\nu} \sum_{\kappa \neq \mu}^{\mathrm{AO}} c_{\kappa\nu} S_{\kappa\mu} \right] \quad (7)$$

where $c_{\mu\nu}$ are the molecular orbital coefficients, AO is the total number of atomic orbitals, $S_{\kappa\mu}$ is the atomic orbital overlap matrix, and ν indicates the frontier molecular orbital HOMO or LUMO as defined before. In addition, the radical Fukui function condensed to atom *i* is given by

$$f_i^{\mathrm{rad}} = \frac{(f_i^{\mathrm{HOMO}} + f_i^{\mathrm{LUMO}})}{2} \quad (8)$$

The condensed FF's have been found to be a reliable tool in the interpretation of a wide variety of problems.[38] Given that f_i^{HOMO} provides a quantitative index of the susceptibility of atom *i* toward electrophilic attacks, we calculate these indices for the reactions M + nFe$^{\mathrm{III}}$ (with n = 0, 1, 2). The condensed FF methodology (eqs 7 and 8) has been implemented in a subroutine within a modified version of the Gaussian 03 package.[39] The Fukui functions were computed by performing single-point calculations on the equilibrium geometries previously obtained by the CPMD calculations with the gradient-corrected DFT PBE exchange-correlation functional[40] using the 6-31G** basis (B3LYP/6-31G**//CPMD).

E. Experimental Method. Aqueous solutions were prepared from M (methyl-α-mannopyranoside, Sigma, minimum 99%) and $FeCl_3$ (Sigma Aldrich, 97%).[27] In order to ensure consistency with previous studies,[13,14] we also looked at the complexes of Fe$^{\mathrm{III}}$ with mannose, preparing solutions with D-(+)-mannose (Sigma, ≥99%). Typical concentrations of the carbohydrate were ~1×10^{-5}–5×10^{-5} M, and we explored a broad range of carbohydrate−Fe$^{\mathrm{III}}$ ratios.

Initial mass spectrometric studies were performed with a dual-probe electrospray ion source, including an integrated three-vacuum stage and ion optics assembly (Analytica of Branford), coupled to a custom-built Extrel quadrupole mass spectrometer (Ardara Technologies). In these experiments, ESI was employed solely to characterize the distribution of ions in solution. In subsequent CID experiments, we employed a Micromass Quattro Micro triple quadrupole instrument to measure the fragmentation pathways of the Sac−Fe complexes.

III. Results and Discussion

A. Active Sites of the Carbohydrate. Chemical reactivity calculations using the condensed Fukui functions (see Methods Section) indicate that the O2 and O4 atoms (Figure 1A), with f^{HOMO} values of 0.38 and 0.32, possess strong nucleophilic character (Table 1). The O2 and O4 atoms in the hydroxyl groups are the potential hard bases that react with the hard acid, Fe$^{\mathrm{III}}$, based on the formulation of the acid−base concept of Pearson.[41] In addition, our average natural partial charge analysis (NPA) illustrates that the hydroxyl oxygen atoms have larger partial negative charges than the ring oxygen (O5) and methoxy oxygen (O1) atoms (see Table 2), indicative of a better Lewis base reactivity from hydroxyl group oxygen atoms than that of the methoxy and ring oxygen atoms.

TABLE 1: Calculated Chemical Reactivity Indexes f^{HOMO} Based on Condensed Fukui Functions[a]

atom	A	B
O2	0.38106	0.50533
O3	0.01906	0.01135
O6	0.00153	0.00080
O5	0.01999	0.07802
O4	0.32149	0.07753
O1	0.01602	0.18454

[a](A) methyl-α-D-mannopyranoside and (B) Fe$^{\mathrm{III}}$ and methyl-α-D-mannopyranoside.

TABLE 2: Calculated Average Natural Partial Charges (NPA) for the Metal Ion and the Specific Carbohydrate Atoms Using the BLYP Method and 6-311+G(2d,p) Basis Set[a]

atom	A	B
O1	−0.59 ± 0.06	−0.72 ± 0.03
O2	−0.73 ± 0.04	−0.62 ± 0.05
O3	−0.75 ± 0.04	−0.63 ± 0.04
O4	−0.76 ± 0.05	−0.61 ± 0.06
O5	−0.59 ± 0.04	−0.52 ± 0.03
O6	−0.75 ± 0.03	−0.54 ± 0.07
Fe$^{\mathrm{III}}$		+1.77 ± 0.08

[a] Trajectories used in NPA calculations belong to the minimum-energy configuration of the glycosidic linkage of the carbohydrate obtained from CPMD simulations for (A) methyl-α-D-mannopyranoside and (B) methyl-α-D-mannopyranoside and one Fe$^{\mathrm{III}}$ Ion. Note that the ± are not uncertainties but give a range for the fluctuations around the equilibrium values. These were determined via the time-dependent standard deviation method.

CPMD simulations with one Fe$^{\mathrm{III}}$ ion and M show that the Fe$^{\mathrm{III}}$ ion is coordinated to the O2, O3, and O4 atoms (Figure 1B) within 25 ps simulations and stays coordinated to these oxygen atoms for the rest of the simulation (45 ps). This finding supports the chemical reactivity index and NPA results, which identified the O2 and O4 atoms as the most active toward the Fe$^{\mathrm{III}}$ ion. According to our CPMD simulations, the distances between Fe$^{\mathrm{III}}$ and the O2, O3, and O4 atoms (Figure 1B) vary between 2.7 and 3.8 Å, and the average O2−Fe$^{\mathrm{III}}$−O4 angle is such that the transition-metal ion is symmetrically placed between the O2 and O4 atoms (see Table 3). In contrast, classical MD simulations did not reproduce these specific interactions. Classical simulations indicate a more-mobile and less-coordinated Fe$^{\mathrm{III}}$; its distance to all hydroxyl oxygen atoms of the carbohydrate varies between 5 and 11 Å. This might be because classical simulations (using force field parameters) neglect differences in the hydroxyl oxygen partial charge parameters, fail to distinguish between axial and equatorial orientations of hydroxyl groups, and ignore the conformation dependence of steric factors and their effects on electrostatics.

The conformational details afforded by the CPMD simulations are in very good agreement with our CID experiments. Although we were unable to generate bare $[MFe]^{3+}$ complexes, we performed CID on $[MFeCl_2]^+$ and observed patterns consistent with coordination of Fe$^{\mathrm{III}}$ to O2, O3, and O4. We note that CID was also performed on $[MFeCl]^+$ and $[M_2FeCl]^+$, and the results were in agreement with those reported by Carlesso et al.[13,14] The major fragmentation pathways involve H_2O, CH_3OH, or $C_3H_6O_2$ losses; subsequent H_2O losses are observed from each of the initial fragments, and at higher collision energies, it appears that FeCl is lost so that the fragmentation pattern resembles that for bare $[MH]^+$. As Figure 2 shows, selection

TABLE 3: Specific Bond Lengths and Bond Angles of Methyl-α-D-mannopyranoside and Its Complexes with Fe^{III} Ions Calculated via CPMD and Classical MD Simulations[a]

	A		B		C	
	CPMD	MD	CPMD	MD	CPMD	MD
O3−H2/Å	2.0 ± 0.3	2.3 ± 0.5	2.3 ± 0.2	2.5 ± 0.4	2.7 ± 0.2	2.9 ± 0.4
O4−H3/Å	2.4 ± 0.4	2.7 ± 0.5	2.5 ± 0.2	2.7 ± 0.3	2.4 ± 0.3	2.9 ± 0.2
O6−H4/Å	2.1 ± 0.3	2.9 ± 0.4	2.5 ± 0.2	2.7 ± 0.2	2.4 ± 0.3	3.2 ± 0.4
θ(O2H2O3)/degrees	146 ± 19	107 ± 23	109 ± 17	116 ± 38	106 ± 18	108 ± 39
θ(O3H3O4)/degrees	112 ± 28	101 ± 21	103 ± 13	101 ± 25	106 ± 10	98 ± 19
θ(O4H4O6)/degrees	120 ± 27	115 ± 38	100 ±± 22	129 ± 28	105 ± 14	117 ± 31
Fe^{III}_A−O2/Å			3.3 ± 0.2	8.4 ± 3.2	3.3 ± 0.2	8.7 ± 2.9
Fe^{III}_A−O3/Å			3.0 ± 0.3	7.9 ± 2.2	3.9 ± 0.2	8.8 ± 3.1
Fe^{III}_A−O4/Å			3.5 ±± 0.3	7.7 ± 3.5	4.1 ± 0.5	8.2 ± 3.6
θ(O2FeO4)/degrees			69 ± 4		68 ± 3	
Fe^{III}_B−O1/Å					5.1 ± 1.9	7.3 ± 3.2
Fe^{III}_B−O2/Å					4.9 ± 1.4	9.8 ± 2.1

[a] Atom numbers listed here are illustrated in Figure 1A−D: methyl-α-D-mannopyranoside (A), one Fe^{III} ion and methyl-α-D-mannopyranoside (B), and two Fe^{III} ions and methyl-α-D-mannopyranoside (C). Fe^{III}_A and Fe^{III}_B present the first and second iron ions, respectively.

of the Fe^{III} complex, $[MFeCl_2]^+$, yields a slightly different pattern. CH_3OH and HCl loss are competitive at low energies, and sequential loss proceeds facilely irrespective of order (first evident at 7 V collision energy). Only at higher collision energies (~ 20 V) are H_2O losses from $[MFeCl_2-HCl-CH_3OH]^+$ seen. At collision energies ≥14 V, the CID spectrum is dominated by a peak pattern consistent with $FeCl_2$ loss from $[MFeCl_2]^+$, followed by molecular fragmentation. It is the low-energy results, however, that provide valuable insights into the structure of the complex by indicating Fe^{III} coordination to O2, O3, and O4. The CID spectrum of any pyranoside is expected to exhibit CH_3OH loss,[15] but uncomplexed M subsequently (and competitively) loses H_2O. Because the hydroxyl oxygen atoms are "protected" via their interaction with Fe^{III}, only at much higher collision energies does the H_2O-loss pattern—so commonly observed with saccharides—appear. Therefore, while the Cl atoms likely play a significant role in the coordination of $FeCl_2$ to M, we are confident that coordination occurs at all three of the hydroxyl oxygen atoms. Thus, the CID experiments indicate complex coordination consistent with the specific motif predicted by CPMD simulations.

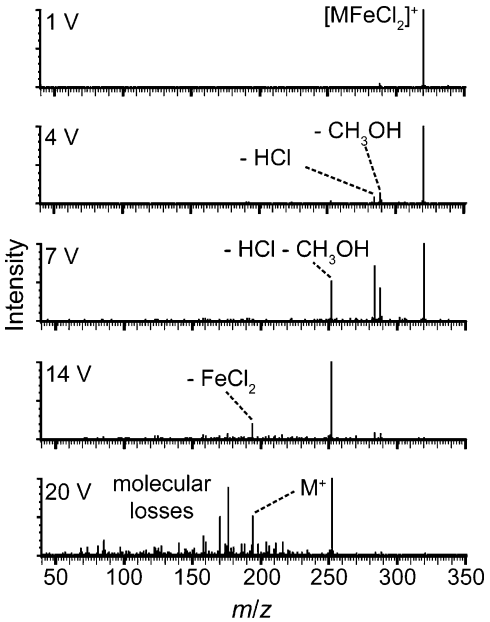

Figure 2. Electrospray ionization mass spectra obtained by selecting the $[MFeCl_2]^+$ ion (where M = methyl-α-D-mannopyranoside) and colliding with Ar gas. The collision energy is noted with each spectrum, and the major fragment channels are labeled.

To study the interaction of the carbohydrate with more than one Fe^{III} ion, we calculated the chemical reactivity index of each atom in the vicinity of an Fe^{III} ion and simulated the M with two Fe^{III} ions (Figure 1C). Results obtained by chemical reactivity index calculations using condensed Fukui functions indicate that the second Fe^{III} ion could be coordinated to the hydroxyl group O2 atom and to the glycosidic linkage O1 atom (Table 1), with f^{HOMO} values of 0.50 and 0.18. CPMD simulations also indicate that the second Fe^{III} ion is closer in distance to O2 and O1 atoms in comparison to the distances between the second Fe^{III} ion and the rest of the heavy atoms. Furthermore, results show that the distances between the second Fe^{III} and possible coordination sites on the carbohydrate are larger than those obtained for a single Fe^{III} ion and active carbohydrate sites (Table 3). This finding indicates that the second Fe^{III} is bound more weakly than the first. Classical MD simulations overestimate the mobility of the Fe^{III} ion in comparison to CPMD simulation results (Table 3).

To further evaluate the probability of the first and second Fe^{III} coordination to the carbohydrate, we calculated the binding energies for each of these Fe^{III} ions using the CPMD trajectories and the following relationship

$$A + B \rightarrow AB$$
$$BE = E_{AB} - E_A - E_B \quad (9)$$

where BE represents the binding energy and A and B represent the Fe^{III} ion and M, respectively. According to these calculations, the coordination of the first Fe^{III} ion yields a BE value of −164.2 kJ mol^{-1}, which indicates a preferred interaction between a single Fe^{III} ion and the carbohydrate. On the other hand, the computed BE for the coordination of the second Fe^{III} ion is +328.6 kJ mol^{-1}, indicating that the coordination of a second Fe^{III} ion is energetically unfavorable. Corrections for basis set superposition error (BSSE) was not included in our calculations, which may result in an overestimation of the BEs; trends in BE, however, should not be affected. Overall, these BEs agree with our structural results gained from CPMD simulations, which show larger Fe^{III}-to-carbohydrate distances for the second Fe^{III} ion compared to the values for the complexation of the first Fe^{III} ion.

These findings are consistent with experiment. In fact, even at 1:20 M−Fe^{III} ratios, the ESI experiments found no more than one Fe coordinated to the carbohydrate. These findings are also in good agreement with those of Carlesso et al.,[13,14] who noted that the major species in the mass distribution (their studies

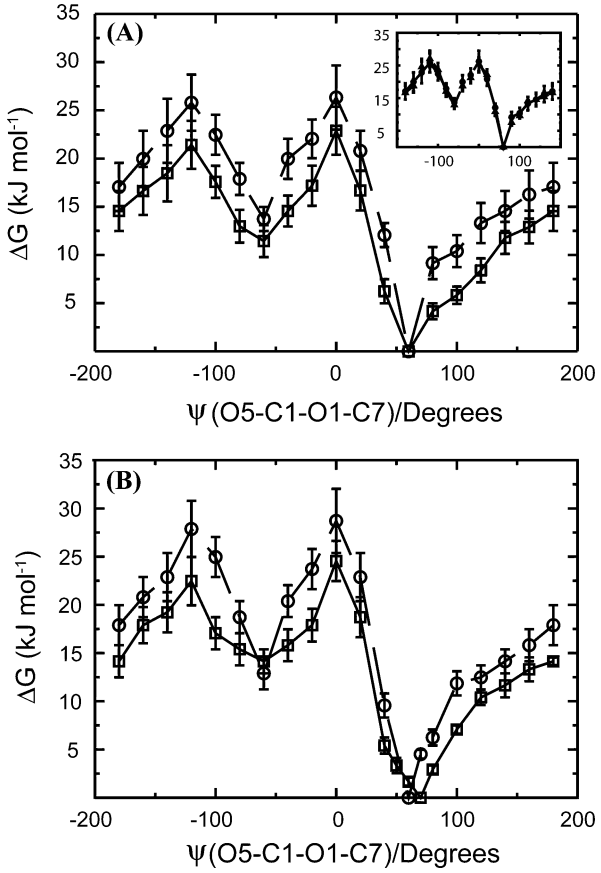

Figure 3. Calculated torsional energy change of the glycosidic linkage of methyl-α-D-mannopyranoside (A) and its energy change in the vicinity of one Fe^{III} ion (B), with the potential of mean force method: (solid line, squares) classical MD simulations, (dashed line, circles) CPMD simulations. The inset plot (A) presents the calculated energy differences of the glycosidic linkage of methyl-α-D-mannopyranoside with the perturbation and potential of mean force methods by classical MD simulations. Errors were calculated utilizing the time-dependent standard deviation method.

involved $FeCl_2$ but our spectra consistently exhibited a strong resemblance to theirs) actually correspond to multiple mannose coordination to one Fe and not vice versa.

B. Glycosidic Linkage Flexibility. The relative torsional energies of the glycosidic linkage (φ) of M (Figure 1A) were studied using CPMD and classical MD simulations in the gas phase. Changes arising in PMF as a function of the torsional angle derived from these calculations are presented in Figure 3A. Similar trends for the conformational preference of the glycosidic linkage of M are observed both by CPMD and classical MD simulations via PMF calculations: g+ > t > g−. Furthermore, the obtained difference regarding the glycosidic linkage flexibility of the saccharide is between 2 and 9% utilizing PMF and perturbation method calculations (Figure 3A). This deviation is in agreement with results obtained recently for the torsional relative energies of methyl-β-mannose in an aqueous solution using the same theoretical techniques.[22]

The interaction with the Fe^{III} ion impacts the preferred conformation of the glycosidic linkage of M; the PMF minimum shifts from 60 to 70°, and the obtained trend in PMF via CPMD simulations becomes g+ > t ≈ g− (Figure 3B). According to the classical MD simulations, the presence of the Fe^{III} ion does not affect the predicted PMF for the glycosidic linkage of the methyl-α-D-mannopyranoside (see Figure 3B). Overall, these results not only show the differences in coordination chemistry (see above) but also the differences in thermodynamic information obtained via classical MD and CPMD simulations.

C. Hydrogen-Bonding Properties. According to our CPMD simulations, the average intramolecular hydrogen bond distances between O2 and O3, O3 and O4, and O4 and O6 (Figure 1A) for M vary between 1.7 and 2.8 Å, whereas these intramolecular hydrogen bond distances are between 1.8 and 3.3 Å with the classical MD simulations (Table 2). Even though the distance OH−O has been used in the literature as a criterion for defining hydrogen bonds, the bond angle, O−H−O, plays an important role too. Encouraged by CPMD simulation results presented by Molteni and Parrinello for glucose and by Coskuner for methyl-β-mannose in water, we set the angular criterion to values larger than 120° for the intramolecular O−H−O angle.[22,23] According to this criterion, we find hydrogen bonds between O2 and O3, and O4 and O6 atoms for M for each trajectory obtained by CPMD simulations (Table 3). This finding is in partial agreement with the studies of Molteni and Parrinello,[24] who reported intramolecular hydrogen bonds between O4 and O6 atoms for glucose, and our results indicate that these bonds do not show dependence on the structure of mannose and glucose, that is, the equatorial or axial orientation of the O2 atom does not affect the existence of these intramolecular hydrogen bonds.

Short-lived hydrogen bonds between the O4 and O6 atoms were discussed recently for methyl-β-mannose utilizing CPMD simulations, indicating that the axial or equatorial orientation of the glycosidic linkage does not affect the presence of this bond. These structural properties could not be demonstrated by classical MD simulations (Table 3). For the g+ orientation of the glycosidic linkage of M, we find intramolecular hydrogen bonds between O2 and O3, O3 and O4, and O4 and O6 atoms via CPMD simulations. On the other hand, for the g− and t orientations of the glycosidic linkage of the carbohydrate, we observe no hydrogen bonds between the O2 and O3 atoms. This finding might indicate that the intramolecular hydrogen bonds observed between O2 and O3 atoms for the g+ orientation of the glycosidic linkage stabilizes this conformation over its g− and t orientations. For the t orientation of the glycosidic linkage, the hydrogen bond between O3 and O4 atoms is 23% shorter-lived in comparison to that for its g− orientation. This finding is indicative of the role of hydrogen bonding between O3 and O4 atoms in stabilizing the g− orientation of the linkage over its t orientation.

In the vicinity of a single Fe^{III} ion, the intramolecular hydrogen bond between O2 and O3 atoms, reported for M, diminishes according to our CPMD simulations. Short-lived intramolecular hydrogen bonds were observed between the O4 and O6 atoms. These results show that the interaction of the carbohydrate with a metal cation impacts the predicted hydrogen bonding. The average number of intramolecular hydrogen bonds remained low, even if the criteria for selecting intramolecular hydrogen bonds were changed by lowering the threshold O−H−O angle to 100°. However, a second intramolecular hydrogen bond between O2 and O3 atoms exists when we change the criterion by increasing the intramolecular hydrogen-bond distance up to 2.7 Å via CPMD simulations. For the g+ orientation of the glycosidic linkage of M, which is coordinated to a single Fe^{III} ion, we observed intramolecular hydrogen bonds between O2 and O3 and O4 and O6 atoms. The hydrogen bond between O2 and O3 atoms diminished for the g− and t orientations. This result indicates that the hydrogen bond between O2 and O3 atoms stabilizes the g+ orientation of the glycosidic linkage over its g− and t orientations.

One reason for the discrepancy in results obtained by classical MD simulations is that the partial charge on oxygen atoms changes with the coordination of a trivalent metal ion, as shown in natural partial charge analysis (Table 2). However, most force field parameters for classical simulations do not capture these changes in the details of the electrostatics.

Overall, the inclusion of many-body interactions by force field parameter-free CPMD simulations provides a different means of studying the coordination of metal ions to a carbohydrate. In CPMD, the electronic and nuclear degrees of freedom are treated as a system of coupled equations of motion. This allows efficient dynamics simulations to be performed with a high-quality potential computed at each time step. We should mention that the differences between results obtained for M are small, but the differences in structural and thermodynamic properties increase in the presence of a transition-metal ion. Furthermore, classical MD and CPMD simulations give different results concerning the coordination of the metal ion to the carbohydrate. Differences obtained between CPMD and classical MD simulation results might also indicate that better force field parameters for Fe^{III} and cross parameters for Fe^{III} and carbohydrates are required. Differences in determined structures also impact the chemical reactivity of the carbohydrate toward Fe^{III}. We notice that computed intramolecular hydrogen bonds for the carbohydrate differ from each other via classical and CPMD simulations. This result is in agreement with the recent theoretical studies of methyl-β-mannose.[22]

IV. Conclusion

We have used an integrated approach based on theoretical calculations, mass spectrometric measurements, natural partial charge analysis, and molecular dynamics simulations to predict the active sites of a biomolecule toward metal ions. Results were compared to those obtained via classical MD simulations. The insights obtained from the CPMD simulations are in agreement with the chemical reactivity index calculations and proved to be consistent with mass spectrometric measurements.

Our theoretical studies at the ab initio level indicate that more than one hydroxyl oxygen atom coordinates to the Fe^{III} ion, and our simulations and binding energy calculations indicate that the coordination of a single Fe^{III} ion is more likely than the coordination of two Fe^{III} ions to a M. Experimental observations agree insofar as multiple uptake of M onto Fe^{III} is ubiquitous while multiple uptake of Fe^{III} onto M is not seen.

In addition, coordination with a metal ion impacts the preferred glycosidic linkage conformation of the saccharide based on our CPMD simulations. The glycosidic linkage preference changes from g+ > g− > t to g+ > g− ≈ t in the presence of an Fe^{III} ion. CPMD simulations clearly demonstrate that the preference of a g+ conformation is due to intramolecular hydrogen bonding. We also conclude that the chemical reactivity of a carbohydrate toward a metal ion is defined by steric factors, including intramolecular hydrogen bonding. We further demonstrated that our classical MD simulations are insensitive to these important chemical properties.

This study indicates that first-principles studies (condensed Fukui functions and CPMD simulations) and complementary mass spectrometry studies can provide insights into the structure and function of organometallic complexes. Currently, we are applying these techniques to the coordination of metal ions to carbohydrates in aqueous solution and to the coordination of transition-metal ions to peptides and proteins, and we are confident that validated first-principles techniques will help to predict the reaction mechanisms of physiological processes such as receptor and ligand binding in which metal−organic complexes play crucial roles.

Acknowledgment. The authors thank T. C. Allison, E. Bylaska, and Y. Simon-Manso for helpful discussions. We thank P. Neta for experimental assistance.

References and Notes

(1) Best, T.; Kemps, E.; Bryan, J. *Nutr. Neurosci.* **2007**, *10*, 113.
(2) West, A. R.; Oates, P. S. *Am. J. Physiol.: Gastrointest. Liver Physiol.* **2005**, *289*, G1108.
(3) Horak, D.; Babic, M.; Jendelova, P.; Herynek, V.; Trchova, M.; Pientka, Z.; Pollert, E.; Hajek, M.; Sykova, E. *Bioconjugate Chem.* **2007**, *18*, 635.
(4) Miyoshi, S.; Flexman, J. A.; Cross, D. J.; Maravilla, K. R.; Kim, Y.; Anzai, Y.; Oshima, J.; Minoshima, S. *Mol. Imaging Biol.* **2005**, *7*, 286.
(5) Chan, C. S. C. S.; De Stasio, D.; Welch, S. A.; Girasole, M.; Frazer, B. H.; Nesterova, M. V.; Fakra, S.; Banfield, J. F. *Science* **2004**, *303*, 1656.
(6) Kim, E. J.; Sabra, W.; Zeng, A. P. *Microbiology* **2003**, *149*, 2627.
(7) Saltman, P. *J. Chem. Educ.* **1965**, *42*, 682.
(8) Spiro, T. G.; Saltman, P. *Struct. Bonding* **1969**, *6*, 116.
(9) Charley, P. J.; Sarkar, B.; Stitt, C. F.; Saltman, P. *Biochem. Biophys. Acta* **1963**, *69*, 313.
(10) Davis, P. S.; Deller, D. J. *Nature* **1966**, *212*, 40.
(11) Rao, P. C.; Geetha, K.; Raghavan, M. S. S.; Sreedhara, A.; Tokunaga, K.; Yamagucchi, T.; Jadhav, V.; Ganesh, K. N.; Krishnamoorthy, T.; Ramalah, K. V. A.; Bhattacharyya, RK. *Inorg. Chim. Acta* **2000**, *297*, 373.
(12) (a) Colton, R.; Harrison, K. L.; Mah, Y. A.; Traeger, J. C. *Inorg. Chim. Acta* **1995**, *231*, 65. (b) Di Marco, V. B.; Bombi, G. G. G. G. *Mass Spectrom. Rev.* **2006**, *25*, 347. (c) Traeger, J. C. *Int. J. Mass Spectrom.* **2000**, *200*, 387.
(13) Carlesso, V.; Fournier, G.; Tabet, J. C. *Eur. J. Mass Spectrom.* **2000**, *6*, 421.
(14) Carlesso, V.; Afonso, C.; Fournier, F.; Tabet, J. C. *Int. J. Mass Spectrom.* **2002**, *219*, 559.
(15) Madhusudanan, K. P.; Kanojiya, S.; Kumar, B. *J. Mass Spectrom.* **2005**, *40*, 1044.
(16) Salpin, J. Y.; Tortajada, J. *J. Mass Spectrom.* **2002**, *37*, 379.
(17) Petrova, P.; Koca, J.; Imberty, A. *Eur. J. Biochem.* **2001**, *268*, 5365.
(18) Krewulak, K. D.; Shepherd, C. M.; Vogel, H. J. *BioMetals* **2005**, *18*, 375.
(19) Silanpaa, A. J.; Aksela, R.; Laasonen, K. *Phys. Chem. Chem. Phys.* **2003**, *5*, 3382.
(20) Best, R. E.; Jackson, G. E.; Naidoo, K. J. *J. Phys. Chem. B* **2001**, *105*, 4742.
(21) Hajduk, P. J.; Horita, D. A.; Kerner, L. E. *J. Am. Chem. Soc.* **1993**, *115*, 9196.
(22) Coskuner, O. *J. Chem. Phys.* **2007**, *127*, 015101.
(23) (a) Coskuner, O.; Jarvis, E. A. A.; Allison, T. C. *Angew. Chem., Int. Ed.* **2007**, *46*, 7853. (b) Coskuner, O.; Jarvis, E. A. A.; Allison, T. C. *Angew. Chem.* **2007**, *119*, 7999.
(24) Molteni, C.; Parrinello, M. *J. Am. Chem. Soc.* **1998**, *120*, 2168.
(25) Coskuner, O.; Jarvis, E. A. A. *J. Phys. Chem. A* **2007**, accepted for publication.
(26) Bylaska, E. J.; de Jong, W. A.; Kowalski, K.; et al. *NWCHEM, A Computational Chemistry Package for Parallel Computers*, version 5.0; Pacific Northwest National Laboratory: Richland, Washington, 2006.
(27) Certain commercial equipment and software are identified in this paper in order to specify the experimental procedure adequately. Such identification is not intended to imply recommendation or endorsement by the National Institute of Standards and Technology nor is it intended to imply that the software or equipment identified are necessarily the best available for the purpose.
(28) Troullier, N.; Martins, J. L. *Phys. Rev. B* **1991**, *43*, 1993.
(29) Lee, C.; Yang, W.; Parr, R. C. *Phys. Rev. B* **1988**, *37*, 785.
(30) Kale, L.; Skeel, R.; Bhandarkar, M.; Brunner, R.; Gursoy, A.; Krawetz, N.; Philips, J.; Shinozaki, A.; Varandarajan, K.; Schulten, K. *J. Comput. Phys.* **1999**, *151*, 283.
(31) Damm, W.; Frontera, A.; Tirado-Rives, J.; Jorgensen, W. L. *J. Comput. Chem.* **1997**, *18*, 1955.
(32) Rappe, A. K.; Casewit, C. J.; Colwell, K. S.; Goddard, W. A., III; Skiff, W. M. *J. Am. Chem. Soc.* **1992**, *114*, 10024.
(33) Allen, M. P.; Tildesley, D. *Computer Simulations of Liquids*; Oxford University Press: New York, 1987.
(34) (a) Parr, R.; Yang, W. *Density Functional Theory of Atoms and Molecules*; Oxford University Press: New York, 1989. (b) Parr, R. G.; Yang, W. *J. Am. Chem. Soc.* **1984**, *106*, 4049. (c) Yang, W.; Parr, R. G.; Pucci,

R. *J. Chem. Phys.* **1984**, *81*, 2862. (d) Yang, W.; Parr, R. G. *Proc. Natl. Acad. Sci. U.S.A* **1985**, *82*, 6723.

(35) Ciosloski, J.; Martinov, M.; Mixon, S. T. *J. Phys. Chem*. **1993**, *97*, 10948.

(36) Senet, P. *J. Chem. Phys*. **1997**, *107*, 2516.

(37) Contreras, R. R.; Fuentealba, P.; Galván, M.; Pérez, P. *Chem. Phys. Lett.* **1999**, *304*, 405.

(38) See, for example: (a) Fuentealba, P.; Contreras, R. R. *Reviews of Modern Quantum Chemistry. A Celebration of the Contributions of Robert G Parr*; World Scientific: Singapore, 2002; p 1013. (b) Chermette, H.; Boulet, P.; Portmann, S. *Reviews of Modern Quantum Chemistry. A Celebration of the Contributions of Robert G Parr*; World Scientific: Singapore, 2002; p 992. (c) Fuentealba, P.; Pérez, P.; Contreras, R. R. *J. Chem. Phys*. **2000**, *113*, 2544. (d) Bulat, F. A.; Chamorro, E.; Fuentealba, P.; Toro-Labbé *J. Phys. Chem. A* **2004**, *108*, 342.

(39) Frisch, M. J.; Trucks, G. W.; Schlegel, H. B.; Scuseria, G. E.; Robb, M. A.; Cheeseman, J. R.; Montgomery, J. J. A.; Vreven, T.; Kudin, K. N.; Burant, J. C.; Millam, J. M.; Iyengar, S. S.; Tomasi, J.; Barone, V.; Mennucci, B.; Cossi, M.; Scalmani, G.; Rega, N.; Petersson, G. A.; Nakatsuji, H.; Hada, M.; Ehara, M.; Toyota, K.; Fukuda, R.; Hasegawa, J.; Ishida, M.; Nakajima, T.; Honda, Y.; Kitao, O.; Nakai, H.; Klene, M.; Li, X.; Knox, J. E.; Hratchian, H. P.; Cross, J. B.; Bakken, V.; Adamo, C.; Jaramillo, J.; Gomperts, R.; Stratmann, R. E.; Yazyev, O.; Austin, A. J.; Cammi, R.; Pomelli, C.; Ochterski, J. W.; Ayala, P. Y.; Morokuma, K.; Voth, G. A.; Salvador, P.; Dannenberg, J. J.; Zakrzewski, V. G.; Dapprich, S.; Daniels, A. D.; Strain, M. C.; Farkas, O.; Malick, D. K.; Rabuck, A. D.; Raghavachari, K.; Foresman, J. B.; Ortiz, J. V.; Cui, Q.; Baboul, A. G.; Clifford, S.; Cioslowski, J.; Stefanov, B. B.; Liu, G.; Liashenko, A.; Piskorz, P.; Komaromi, I.; Martin, R. L.; Fox, D. J.; Keith, T.; Al-Laham, M. A.; Peng, C. Y.; Nanayakkara, A.; Challacombe, M.; Gill, P. M. W.; Johnson, B.; Chen, W.; Wong, M. W.; Gonzalez, C.; Pople, J. A. *Gaussian 03*, Revision C.02; Gaussian, Inc: Wallingford, CT, 2004.

(40) (a) Perdew, J. P.; Burke, K.; Ernzerhof, M. *Phys. Rev. Lett.* **1996**, *77*, 3865. (b) Perdew, J. P.; Burke, K.; Ernzerhof, M. *Phys. Rev. Lett.* **1997**, *78*, 1396.

(41) Pearson, R. G. *J. Am. Chem. Soc.* **1963**, *85*, 3583.